

## High-pressure synthesis of the BiVO<sub>3</sub> perovskite

R. A. Klein,<sup>1</sup> A. B. Altman,<sup>1</sup> R. J. Saballos,<sup>2</sup> J. P. S. Walsh,<sup>1</sup> A. D. Tamerius,<sup>1</sup> Y. Meng,<sup>3</sup> D. Puggioni,<sup>2</sup> S. D. Jacobsen,<sup>4</sup> J. M. Rondinelli,<sup>2</sup> and D. E. Freedman<sup>1</sup>

<sup>1</sup>*Department of Chemistry, Northwestern University, Evanston, Illinois 60208, USA*

<sup>2</sup>*Department of Materials Science and Engineering, Northwestern University, Evanston, Illinois 60208, USA*

<sup>3</sup>*HPCAT, X-ray Science Division, Argonne National Laboratory, Lemont, Illinois 60439, USA*

<sup>4</sup>*Department of Earth and Planetary Sciences, Northwestern University, Evanston, Illinois 60208, USA*



(Received 4 March 2019; published 20 June 2019)

We report the high-pressure, high-temperature synthesis of BiVO<sub>3</sub>, a cubic perovskite that thus far has remained inaccessible under ambient pressure conditions. We created this material at ~25 GPa and 1500 K in a laser-heated diamond-anvil cell and recovered it to ambient pressure and temperature. Our synthetic approach circumvents the oxidative chemistry that, at ambient pressures, previously rendered the cubic BiVO<sub>3</sub> perovskite inaccessible. We find through density-functional theory calculations that this material is a unique metallic and antiferromagnetic transition-metal oxide.

DOI: [10.1103/PhysRevMaterials.3.064411](https://doi.org/10.1103/PhysRevMaterials.3.064411)

Perovskites are ubiquitous in our planet and society. They are one of the primary mineral phases in the Earth's mantle [1–3], the structural foundation for cuprate superconductors [4–6], and platforms for a new class of photovoltaics [7,8]. This extremely broad range of applications stems from the vast chemical and structural variation possible in the simple ABX<sub>3</sub> formula. The A, B, and X sites are all easily chemically substituted. As such, perovskites are ideal platforms for the rational design of materials with specific, tailored magnetic and electronic functionality via chemical substitution. The ability to design perovskites has led to the realization of materials that are extremely promising candidate photovoltaics [7,9], photocatalysts [10,11], and multiferroics [12,13].

The family of bismuth–first-row transition-metal oxide perovskites, BiMO<sub>3</sub>, exhibits particularly intriguing behavior ( $M = \text{Sc, Cr, Mn, Fe, Co, Ni}$ ) [14–19]. For example, in BiMnO<sub>3</sub>, the stereochemically active lone pair of electrons belonging to Bi is argued to give rise to (anti)ferroelectric behavior. Simultaneously, the electronic spins on the Mn ions couple ferromagnetically, making BiMnO<sub>3</sub> a magnetoelectric multiferroic [20–22].

The family of BiMO<sub>3</sub> perovskites is almost complete. To date, only the perovskites with  $M = \text{Ti}^{3+}$  and  $\text{V}^{3+}$  remain undiscovered. Targeting BiVO<sub>3</sub> is particularly promising due to previous theoretical studies which suggest it may exhibit multiferroic behavior and that it may be an efficient, visible light-driven photocatalyst for water oxidation due to its band gap and optical absorption properties [23,24]. While a thin film of BiVO<sub>3</sub> was recently reported [25], bulk, crystalline BiVO<sub>3</sub> remains synthetically inaccessible at ambient pressure because the Bi<sup>3+</sup> ions preferentially oxidize the V<sup>3+</sup> ions to form V<sup>5+</sup> species and Bi<sup>0</sup> metal [16,26,27].

High-pressure synthesis is a powerful technique ideal for isolating metastable phases of matter [28–33]. High applied pressures transform potential-energy landscapes and allow for the isolation of phases that, under ambient pressures, are inaccessible metastable products [34,35]. Indeed, the

application of high pressures enabled the discovery of several perovskites [36–42]. Therefore, we hypothesized that high applied pressure may shift the thermodynamic landscape in the Bi-V-O system to favor the formation of BiVO<sub>3</sub>.

Herein, we utilize *in situ* powder x-ray diffraction (PXRD) coupled with high-pressure and -temperature conditions in a laser-heated diamond-anvil cell (LHDAC) to synthesize the elusive BiVO<sub>3</sub> perovskite at ~25 GPa and 1500 K. This study demonstrates that the perovskite forms in the cubic  $Pm\bar{3}m$  space group and that it is recoverable to ambient conditions after decompression and thermal quenching. We perform density-functional theory (DFT) calculations and show that the perovskite is simultaneously antiferromagnetic and metallic, and we briefly discuss this rare magnetic and electronic structure predicted for BiVO<sub>3</sub>.

For the synthesis, we pressed the Bi<sup>0</sup> and V<sub>2</sub>O<sub>5</sub> reagents into a flake and loaded the flake in a DAC [43]. We pressurized the sample to 25.1(5) GPa and then laser heated to ~1550 K at beamline 16-ID-B (HPCAT, Advanced Photon Source, Argonne National Laboratory) using infrared lasers [44]. We utilized *in situ* PXRD, which is an especially effective technique when paired with high-pressure synthesis as it provides time-resolved characterization of crystalline solid-state products. The use of a two-dimensional (2D) detector enabled phase analysis via the polycrystalline texture of the diffraction rings. Uniform rings of intensity indicate randomly oriented powders while rings of individual spots indicate a collection of randomly oriented submicron-size single crystals, with a higher degree of polycrystalline texture. An analysis of the polycrystalline texture allowed different materials that contribute to a single pattern to be distinguished.

As we heated beyond ~1200 K, Bragg peaks formed in the integrated diffraction patterns, corresponding to rings of individual spots in the 2D detector images (Fig. 1). We held the temperature between 1200 and 1250 K for ~3.5 min, during which time the peaks grew in intensity (Fig. S7, discussed in the Supplemental Material [43]). Once the peaks

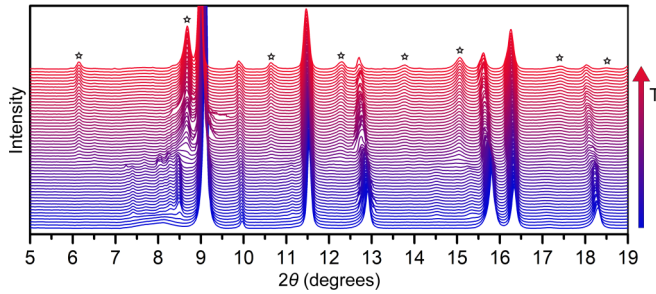


FIG. 1. Bragg peaks from the phase appear in the PXRD patterns after heating the Bi-V-O sample at high pressure ( $\lambda = 0.406\ 63\ \text{\AA}$ ). The temperature increases as indicated by the color of the patterns and by the colored arrow (red is high temperature). Stars mark the position of the peaks. During the heating process, the recrystallization of Bi leads to unphysical saturation features in select patterns.

were no longer increasing in intensity, we rapidly increased the temperature to  $\sim 1450\ \text{K}$ . At  $1400\ \text{K}$ , the first set of peaks promptly disappeared and, simultaneously, a second set of peaks grew in. These peaks manifested in the 2D detector images as smooth rings of intensity evenly distributed across the azimuth. The second set of peaks then grew in intensity in the patterns as we slowly increased the temperature between  $1450$  and  $1550\ \text{K}$  over  $\sim 6.5$  min, after which time the peaks no longer changed intensity. We then thermally quenched the reaction. The second set of peaks retained their intensity after the thermal quench. By the end of the heating experiment, the pressure had dropped to  $21.4(5)$  GPa.

The time-resolved, *in situ* nature of the experiment was crucial for distinguishing between phases in the 2D detector images. The fact that we observed a set of peaks appearing concurrently at a specific time (and therefore a specific temperature and pressure) allowed us to attribute these peaks to the same phase. The observation that these peaks subsequently grew in intensity at the same rate, along with the shared morphology of their Bragg peaks as observed in the plot of azimuthal intensity in  $2\theta$  space (Fig. S1, top), further supported this interpretation. These observations together suggested that the first set of peaks (between  $1200$  and  $1400\ \text{K}$ ) corresponded to one distinct phase while the second set of peaks (above  $1400\ \text{K}$ ) belonged to a second phase.

We attempted to index both phases. Unfortunately, we were unable to index the first set of peaks we observed between  $1200$  and  $1400\ \text{K}$ , perhaps in part due to the weak diffraction from this phase coupled with the highly nonuniform polycrystalline texture in the 2D detector images. However, we successfully indexed the higher-temperature phase using the TOPAS software package [45]. At high pressure, the peaks indexed to the cubic  $Pm\bar{3}m$  space group, the aristotype space group for perovskites [46–48]. To test whether the observed phase was the targeted  $\text{BiVO}_3$  perovskite, we performed a Rietveld refinement on the patterns between  $2\theta$  values of  $3^\circ$  and  $22^\circ$  (Fig. 2) [49]. In the refinements, we included the appropriate bismuth polymorph [50],  $\text{MgO}$ , and the  $Pm\bar{3}m$  phase. The  $Pm\bar{3}m$  phase comprised 13 distinct peaks in this  $2\theta$  range with a powdery polycrystalline texture. In addition, we also observed a set of weak peaks—only observed after thermal quenching and removal of the heating apparatus—that were not modeled by our Rietveld analysis. We hypoth-

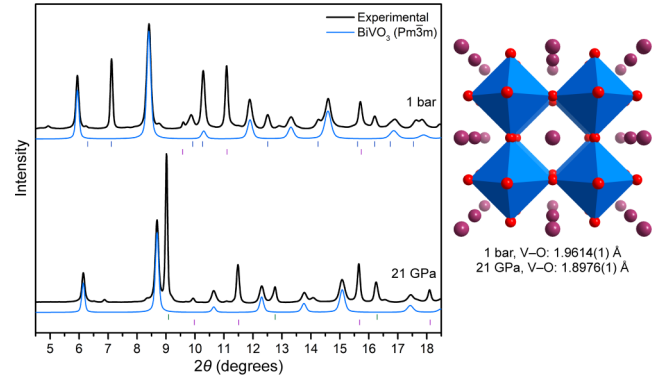


FIG. 2. Rietveld refinements at  $\sim 21.1$  GPa and at ambient pressure (left,  $\lambda = 0.406\ 63\ \text{\AA}$ ) yield the structure of the phase to be the cubic  $\text{BiVO}_3$  perovskite (right). Beneath the patterns, magenta tick marks denote peaks from the crystalline  $\text{MgO}$ , green marks denote peaks from the  $\text{Bi(V)}$  phase at  $21.1$  GPa, and blue marks denote peaks from the  $\text{Bi(I)}$  phase. The structure comprises Bi atoms, O atoms, and  $\text{VO}_6$  moieties (represented as purple and red spheres and as blue octahedra, respectively).

esize they may arise from a minority oxide phase formed in the cooler tail of the laser-heating spot during the heating reaction. These peaks are distinct from the  $Pm\bar{3}m$  phase both temporally and in terms of the crystalline morphology in the 2D detector images. Unfortunately, the weak nature of these peaks precluded indexing. The Rietveld refinement using the cubic  $\text{BiVO}_3$  phase reproduced the observed intensities well.

Once synthesized, we sought to determine if the  $\text{BiVO}_3$  perovskite was stable at ambient pressure and temperature conditions. Towards that end, we obtained PXRD patterns as we slowly decompressed the sample while at ambient temperature [51]. In the diffraction patterns, all of the peaks from the  $\text{BiVO}_3$  phase persist across the entire range of pressures, and all of the Bragg peaks consistently shift with pressure without significant changes in relative intensity. In addition, we fit these data and obtained the second-order Birch-Murnaghan equation of state for  $\text{BiVO}_3$  (Supplemental Material, Figs. S4, S5, Tables S8, S9). The bulk modulus of  $\text{BiVO}_3$  is  $165(4)$  GPa, consistent with the calculated parameters for similar perovskites [52–54].

The perovskite exhibits vertex-sharing  $\text{VO}_6$  octahedra spaced by  $\text{Bi}^{3+}$  ions in the A-cation position. In general, the crystal symmetry for  $A^{3+}B^{3+}\text{O}_3$  perovskites may be predicted based on the ionic radii of A and B [55–57]. The ionic radii of the ions are related by the Goldschmidt tolerance factor  $t$ , such that the perovskite is expected to be cubic when  $0.9 \lesssim t \lesssim 1.0$  [57]. For  $\text{BiVO}_3$ ,  $t = 0.895$  based on the ambient pressure ionic radii for  $\text{V}_{\text{VI}}^{3+}$ ,  $\text{Bi}_{\text{VIII}}^{3+}$ , and  $\text{O}_{\text{II}}^{2-}$  (the subscript roman numeral indicates the ion's coordination number) [55]. We were not able to find detailed ionic radius information for  $\text{Bi}_{\text{XII}}^{3+}$  in the literature. Additionally, the ions' ionic radii decrease with increasing pressure at different rates [34]. The ionic radius of  $\text{Bi}^{3+}$  decreases more rapidly with increasing pressure than does the  $\text{V}^{3+}$  radius. This manifests in the pressure-induced changes in the V–O bond distance and the Bi–O contact distance (Fig. S6). The V–O bond distance decreases by  $\sim 6.4(1)$  picometers (pm) as pressure increases from ambient pressure to  $21.1(5)$  GPa, and the Bi–O contact

distance decreases by  $\sim 9.0(1)$  pm over the same pressure interval. While these distances are affected by the nature of the cation–oxygen bonding, the cations’ radii still change size significantly over this pressure interval [34]. Therefore, as pressure increases, we hypothesize that  $t$  increases and satisfies the requirement for cubic symmetry. And, although the ambient pressure value is right on the verge of a noncubic  $t$  value, we hypothesize that the metastable cubic phase is kinetically trapped at ambient pressure.

Using density-functional theory calculations, we investigated the magnetic and electronic properties of  $\text{BiVO}_3$ . We used the Vienna *Ab initio* Software Package (VASP) with the projected-augmented wave method potentials [58,59], and the recently developed Strongly Constrained and Appropriately Normed (SCAN) meta-Generalized Gradient Approximation (GGA) functional [60]. Our calculations suggest that the *A*-type antiferromagnetically ordered structure (*A*-AFM), with  $q = (0, 0, 1) \pi/a$ , is low in energy when compared to other magnetic orderings, with the paramagnetic phase being  $\sim 16$  meV per formula unit higher in energy (Table S14). We found a local magnetic moment of  $1.51 \mu_B$  on the V atom. The relaxed lattice parameter differs by only  $-1.01\%$  with respect to the experimental value ( $3.88 \text{ \AA}$ ). There have been reports that suggest that the accuracy of the SCAN functional suffers when describing magnetism in the transition metals [61,62]. To assess the accuracy of the SCAN functional in our calculations, we also conducted calculations using the PBESOL (+ $U$ ) method. We found that both functionals predict a metallic antiferromagnetic ground state. The notable difference between the results is that the value of  $U$  stabilizes either the *C*-type or *A*-type AFM ordering (Fig. S20) while maintaining the metallic character.

Our calculations show that cubic  $\text{BiVO}_3$  is antiferromagnetic and metallic (Fig. 3) with strongly dispersive bands (Fig. S2). This is a highly unusual combination, and suggests this compound is worthy of further investigation. Usually, undoped, magnetic transition-metal oxides fall into two categories: semiconducting antiferromagnets and metallic ferromagnets [63,64]. To the best of our knowledge, there are only a handful of reported metallic antiferromagnetic transition-metal oxides:  $\text{SrCrO}_3$  [36–38],  $\text{CaCrO}_3$  [39,40],  $\text{Ca}_3\text{Ru}_2\text{O}_7$  [65],  $\text{LaNiO}_3$  [41],  $\text{LaCu}_3\text{Cr}_4\text{O}_{12}$  [42],  $\text{RuO}_2$  [66,67], and  $(\text{La, Sr})_3\text{Mn}_2\text{O}_7$  [68]. In  $\text{LaCrO}_3$  and  $\text{SrCrO}_3$ , it is proposed that the antiferromagnetism is stabilized by orbital ordering, which lowers the symmetry of the system and lifts the degeneracy of the Cr  $t_{2g}$  manifold. Yet, the mechanism for the anomalous antiferromagnetism in these metallic systems remains incompletely understood, and in some cases, the electronic transport properties remain controversial [69–71].

Our DFT calculations using the SCAN functional show that *A*-type AFM ordering, with planes of ferromagnetic spins coupled antiferromagnetically, is the ground-state spin structure for cubic  $\text{BiVO}_3$ . The antialigned 2D ferromagnetic planes in the structure require that the magnetic unit cell exhibits a lower symmetry than the cubic crystal structure. To understand the stability of the coexisting metallicity and *A*-type antiferromagnetism in cubic  $\text{BiVO}_3$  perovskite, we examined in more detail the electronic density of states (DOS) for two spin configurations: the nonmagnetic (NM) and the

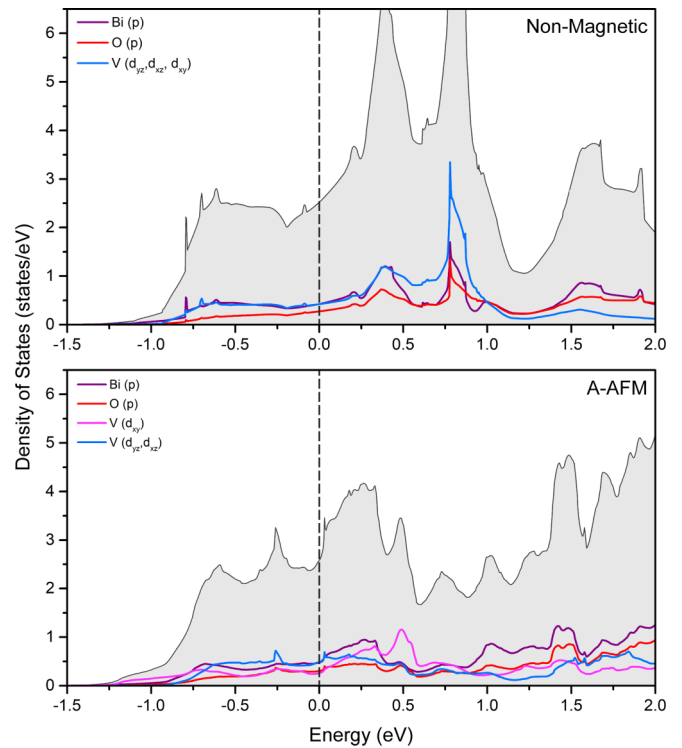


FIG. 3. DOS per formula unit for cubic  $\text{BiVO}_3$  for the nonmagnetic case (top) and for the *A*-type antiferromagnetic ordering case (bottom) both show a nonzero DOS at the Fermi energy. Several van Hove singularities are present in the nonmagnetic DOS diagram above the Fermi energy. In the *A*-AFM DOS, the bands derived from the  $d_{xy}$  orbital are no longer degenerate with those of  $d_{yz}$ ,  $d_{xz}$  symmetry owing to the spin order. The legend indicates the underlying orbital contributions to the total (gray) DOS. The dashed vertical line denotes the Fermi energy.

ground-state *A*-AFM. Near the Fermi level of the NM DOS, we find the presence of several van Hove singularities with a high DOS indicative of a magnetic instability. In contrast, the *A*-AFM DOS shows that the  $t_{2g}$  states split such that the  $d_{xy}$  orbital has a lower occupancy than the degenerate  $d_{xz}, d_{yz}$  doublet leading to orbital polarization (Table S12). In combination with the metallicity of the system, the kinetic energy gain when describing the system using the Stoner model should stabilize itinerant ferromagnetism. However, superexchange originating from the electron localization (well-defined moments exist on the V sublattice) leads to the FM order on  $\{110\}$  planes with adjacent planes exhibiting antialigned spin orientations. Therefore, we attribute the stability of the *A*-type AFM ordering to the competition between superexchange and the itinerant Stoner mechanism [72]. Another factor that might influence the magnetic ordering is the presence of the Bi  $p$  states at the Fermi level, since hybridization of these states with the V  $3d$  orbitals will affect the superexchange pathways. Lastly, the *A*-type and *C*-type ordering are in competition depending on the value of  $U$  in the PBESOL (+ $U$ ) calculations. We acknowledge that it is difficult to unambiguously differentiate between these two similar spin structures.

To assess the importance of spin-orbit coupling on the magnetic and electronic structure of  $\text{BiVO}_3$ , we conducted

a DFT calculation incorporating spin-orbit coupling at the Bi ions using the SCAN functional. We noticed a small decrease in magnetization at the V ions from 1.51 to 1.12  $\mu_B$ ; however, the A-AFM ordering remains stable and the DOS (Fig. S23) shows that the metallicity is retained. We therefore hypothesize that the effects of spin-orbit coupling are minor in this system and that they do not have a significant effect on the magnetic or the electronic properties of BiVO<sub>3</sub>.

In conclusion, we reported the synthesis of the bismuth vanadium oxide perovskite, BiVO<sub>3</sub>. We employed a nontraditional synthetic approach, LHDAC-enabled heating at high-pressure, high-temperature conditions coupled with *in situ* PXRD analysis, to realize this previously inaccessible perovskite. The BiVO<sub>3</sub> perovskite forms in the cubic  $Pm\bar{3}m$  space group when synthesized at high pressures and is recoverable to ambient conditions. The BiVO<sub>3</sub> perovskite expands the known family of bismuth–first-row transition-metal perovskites. We performed density-functional theory calculations and determined that competition between electron delocalization and superexchange favors the A-type or C-type AFM ordering, which might be further enhanced by the anomalous Bi *p* states. We are working to scale up the synthesis of the BiVO<sub>3</sub> perovskite using multianvil press techniques to validate the theoretical prediction of the metallicity concomitant with intrinsic antiferromagnetism in BiVO<sub>3</sub>. We anticipate that a deeper understanding of the origins of these properties in BiVO<sub>3</sub> will help illuminate the underlying physics in the other antiferromagnetic and metallic transition-metal oxides.

Lastly, the need for developing nontraditional synthetic techniques scales with the ever-growing societal and environmental demands for efficient catalytic, photovoltaic, and multiferroic materials. Our work illustrates the utility of high applied pressures for isolating metastable phases which, at ambient pressure, remain thermodynamically unstable and synthetically inaccessible.

The authors thank Dr. S. M. Clarke for insightful discussions. We thank Dr. C. Kenney-Benson, R. Ferry, Dr. X. Chen, and Dr. Y. Li for their invaluable technical support. Experimental work is supported by AFOSR in the form of a PECASE (Grant No. FA9550-17-1-0247). Magnetic studies are supported by the ARO (Grant No. W911NF-18-1-0006 P00001). The collaborative project between D.E.F. and S.D.J. was initiated by Northwestern University (NU) through the Innovative Initiatives Incubator (I3), which supported J.P.S.W. Additionally, S.D.J. acknowledges support from the NSF (Grant No. DMR-1508577), the Capital/DOE Alliance Center (CDAC), and the David and Lucile Packard Foundation. High Pressure Collaborative Access Team (HPCAT) operations are supported by DOE-NNSA's Office of Experimental Sciences. The Advanced Photon Source is a U.S. Department of Energy (DOE) Office of Science User Facility operated for the DOE Office of Science by Argonne National Laboratory under Contract No. DE-AC02-06CH11357. This work made use of the Integrated Molecular Structure Education and Research Center (IMSERC) and the Electronic Probe Instrumentation Center (EPIC) and Keck-II facilities of Northwestern University's Northwestern University Atomic and Nanoscale Characterization Experimental Center (NUANCE), which received support from the Soft and Hybrid Nanotechnology Experimental (SHyNE) Resource (Grant No. NSF ECCS-1542205); the Materials Research Science and Engineering Center (MRSEC) program (Grant No. NSF DMR-1720139) at the Materials Research Center; the International Institute for Nanotechnology (IIN); the Keck Foundation; and the State of Illinois, through the IIN. R.J.S. was supported by the MRSEC at Northwestern University supported by the NSF (Grant No. DMR1720139). D.P. and J.M.R. were supported by the Army Research Office (Grant No. W911NF-15-1-0017) and NSF (Grant No. DMR-1729303), respectively. This work used the Extreme Science and Engineering Discovery Environment (XSEDE) Stampede 2 at the Texas Advance Computing Center through Allocation No. TG-DMR110085.

- [1] A. E. Ringwood, *Geochim. Cosmochim. Acta* **55**, 2083 (1991).
- [2] O. Tschauer, C. Ma, J. R. Beckett, C. Prescher, V. B. Prakapenka, and G. R. Rossman, *Science* **346**, 1100 (2014).
- [3] E. Ito, E. Takahashi, and Y. Matsui, *Earth Planet. Sci. Lett.* **67**, 238 (1984).
- [4] M.-K. Wu, J. R. Ashburn, C. J. Torng, P. H. Hor, R. L. Meng, L. Gao, Z. J. Huang, Y. Q. Wang, and C. W. Chu, *Phys. Rev. Lett.* **58**, 908 (1987).
- [5] C. Chu, L. Gao, F. Chen, Z. Huang, R. Meng, and Y. Xue, *Nature (London)* **365**, 323 (1993).
- [6] J. Orenstein and A. Millis, *Science* **288**, 468 (2000).
- [7] A. Kojima, K. Teshima, Y. Shirai, and T. Miyasaka, *J. Am. Chem. Soc.* **131**, 6050 (2009).
- [8] L. G. Tejuca and J. L. Fierro, *Properties and Applications of Perovskite-type Oxides* (CRC Press, New York, 1992).
- [9] H. J. Snaith, *J. Phys. Chem. Lett.* **4**, 3623 (2013).
- [10] K. Maeda, *J. Photochem. Photobiol., C* **12**, 237 (2011).
- [11] H. Kato and A. Kudo, *J. Phys. Chem. B* **105**, 4285 (2001).
- [12] W. Eerenstein, N. Mathur, and J. F. Scott, *Nature (London)* **442**, 759 (2006).
- [13] D. I. Khomskii, *J. Magn. Magn. Mater.* **306**, 1 (2006).
- [14] A. A. Belik, S. Iikubo, K. Kodama, N. Igawa, S. Shamoto, M. Maie, T. Nagai, Y. Matsui, S. Y. Stefanovich, B. I. Lazoryak, and E. Takayama-Muromachi, *J. Am. Chem. Soc.* **128**, 706 (2006).
- [15] C. Michel, J.-M. Moreau, G. D. Achenbach, R. Gerson, and W. J. James, *Solid State Commun.* **7**, 701 (1969).
- [16] A. A. Belik, *J. Solid State Chem.* **195**, 32 (2012).
- [17] A. A. Belik, S. Iikubo, K. Kodama, N. Igawa, S. Shamoto, S. Niitaka, M. Azuma, Y. Shimakawa, M. Takano, F. Izumi, and E. Takayama-Muromachi, *Chem. Mater.* **18**, 798 (2006).
- [18] S. Ishiwata, M. Azuma, M. Takano, E. Nishibori, M. Takata, M. Sakata, and K. Kato, *J. Mater. Chem.* **12**, 3733 (2002).
- [19] A. A. Belik, *Sci. Technol. Adv. Mater.* **16**, 026003 (2015).
- [20] S.-W. Cheong and M. Mostovoy, *Nat. Mater.* **6**, 13 (2007).
- [21] T. Kimura, S. Kawamoto, I. Yamada, M. Azuma, M. Takano, and Y. Tokura, *Phys. Rev. B* **67**, 180401(R) (2003).
- [22] R. Seshadri and N. A. Hill, *Chem. Mater.* **13**, 2892 (2001).
- [23] C. S. Praveen, L. Maschio, M. Rérat, V. Timon, and M. Valant, *Phys. Rev. B* **96**, 165152 (2017).
- [24] M. K. Yaakob, M. H. Ridzwan, M. F. M. Taib, L. Li, O. H. Hassan, and M. Z. A. Yahya, *J. Appl. Phys.* **125**, 082532 (2019).

- [25] M. Singh and F. Razavi, *AIP Conf. Proc.* **1590**, 90 (2014).
- [26] M. Dragomir and M. Valant, *Ceram. Int.* **39**, 5963 (2013).
- [27] P. Sepiedeh, M. Sc. thesis, Brock University, 2012.
- [28] K. Powderly, S. Clarke, M. Amsler, C. Wolverton, C. Malliakas, Y. Meng, S. Jacobsen, and D. Freedman, *Chem. Commun.* **53**, 11241 (2017).
- [29] C. Darie, C. Goujon, M. Bacia, H. Klein, P. Toulemonde, P. Bordet, and E. Suard, *Solid State Sci.* **12**, 660 (2010).
- [30] S. M. Clarke, M. Amsler, J. P. Walsh, T. Yu, Y. Wang, Y. Meng, S. D. Jacobsen, C. Wolverton, and D. E. Freedman, *Chem. Mater.* **29**, 5276 (2017).
- [31] J. P. S. Walsh, S. M. Clarke, Y. Meng, S. D. Jacobsen, and D. E. Freedman, *ACS Cent. Sci.* **2**, 867 (2016).
- [32] T. Atou, H. Chiba, K. Ohoyama, Y. Yamaguchi, and Y. Syono, *J. Solid State Chem.* **145**, 639 (1999).
- [33] S. M. Clarke, J. P. Walsh, M. Amsler, C. D. Malliakas, T. Yu, S. Goedecker, Y. Wang, C. Wolverton, and D. E. Freedman, *Angew. Chem. Int. Ed.* **55**, 13446 (2016).
- [34] W. Grochala, R. Hoffmann, J. Feng, and N. W. Ashcroft, *Angew. Chem. Int. Ed.* **46**, 3620 (2007).
- [35] L. Zhang, Y. Wang, J. Lv, and Y. Ma, *Nat. Rev. Mater.* **2**, 17005 (2017).
- [36] K.-W. Lee and W. E. Pickett, *Phys. Rev. B* **80**, 125133 (2009).
- [37] L. O. San Martin, A. J. Williams, J. Rodgers, J. P. Attfield, G. Heymann, and H. Huppertz, *Phys. Rev. Lett.* **99**, 255701 (2007).
- [38] A. C. Komarek, T. Moller, M. Isobe, Y. Drees, H. Ulbrich, M. Azuma, M. T. Fernandez-Diaz, A. Senyshyn, M. Hoelzel, G. Andre, Y. Ueda, M. Gruninger, and M. Braden, *Phys. Rev. B* **84**, 125114 (2011).
- [39] A. C. Komarek, S. V. Streltsov, M. Isobe, T. Möller, M. Hoelzel, A. Senyshyn, D. Trots, M. T. Fernández-Díaz, T. Hansen, and H. Gotou *et al.*, *Phys. Rev. Lett.* **101**, 167204 (2008).
- [40] P. A. Bhohe, A. Chainani, M. Taguchi, R. Eguchi, M. Matsunami, T. Ohtsuki, K. Ishizaka, M. Okawa, M. Oura, Y. Senba, H. Ohashi, M. Isobe, Y. Ueda, and S. Shin, *Phys. Rev. B* **83**, 165132 (2011).
- [41] H. Guo, Z. Li, L. Zhao, Z. Hu, C. Chang, C.-Y. Kuo, W. Schmidt, A. Piovano, T. Pi, and O. Sobolev *et al.*, *Nat. Commun.* **9**, 43 (2018).
- [42] T. Saito, S. Zhang, D. Khalyavin, P. Manuel, J. P. Attfield, and Y. Shimakawa, *Phys. Rev. B* **95**, 041109(R) (2017).
- [43] See Supplemental Material at <http://link.aps.org/supplemental/10.1103/PhysRevMaterials.3.064411> for additional experimental and computational details along with raw data and tables.
- [44] Y. Meng, R. Hrubciak, E. Rod, R. Boehler, and G. Shen, *Rev. Sci. Instrum.* **86**, 072201 (2015).
- [45] A. A. Coelho, *TOPAS Academic: General Profile and Structure Analysis Software for Powder Diffraction Data* (Bruker AXS, Karlsruhe, Germany, 2007).
- [46] A. Glazer, *Acta Crystallogr. B* **28**, 3384 (1972).
- [47] C. J. Howard and H. T. Stokes, *Acta Cryst. B* **54**, 782 (1998).
- [48] H. Megaw, *Crystal Structures. A Working Approach (Studies in Physics and Chemistry)* (W. B. Saunders, London, 1973).
- [49] H. Rietveld, *J. Appl. Crystallogr.* **2**, 65 (1969).
- [50] W. Klement Jr, A. Jayaraman, and G. Kennedy, *Phys. Rev.* **131**, 632 (1963).
- [51] Note that while we physically separated the diamonds to achieve zero applied pressure, some residual strain from the solid pressure medium may be possible, such that the perovskite may have experienced slightly above-ambient pressure.
- [52] H. Wang, B. Wang, Q. Li, Z. Zhu, R. Wang, and C. H. Woo, *Phys. Rev. B* **75**, 245209 (2007).
- [53] F. Birch, *Phys. Rev.* **71**, 809 (1947).
- [54] F. Murnaghan, *Proc. Natl. Acad. Sci. USA* **30**, 244 (1944).
- [55] R. D. Shannon, *Acta Crystallogr., Sect. A: Cryst. Phys., Diffraction, Theor. Gen. Crystallogr.* **32**, 751 (1976).
- [56] R. H. Mitchell, M. D. Welch, and A. R. Chakhmouradian, *Mineral. Mag.* **81**, 411 (2017).
- [57] V. M. Goldschmidt, *Naturwissenschaften* **14**, 477 (1926).
- [58] G. Kresse and D. Joubert, *Phys. Rev. B* **59**, 1758 (1999).
- [59] G. Kresse and J. Furthmüller, *Phys. Rev. B* **54**, 11169 (1996).
- [60] J. Sun, A. Ruzsinszky, and J. P. Perdew, *Phys. Rev. Lett.* **115**, 036402 (2015).
- [61] Y. Fu and D. J. Singh, *Phys. Rev. Lett.* **121**, 207201 (2018).
- [62] M. Ekholm, D. Gambino, H. J. M. Jönsson, F. Tasnádi, B. Alling, and I. A. Abrikosov, *Phys. Rev. B* **98**, 094413 (2018).
- [63] J. B. Goodenough and P. M. Raccach, *J. Appl. Phys.* **36**, 1031 (1965).
- [64] J. B. Goodenough, *Prog. Solid State Chem.* **5**, 145 (1971).
- [65] Y. Yoshida, S.-I. Ikeda, H. Matsuhata, N. Shirakawa, C. H. Lee, and S. Katano, *Phys. Rev. B* **72**, 054412 (2005).
- [66] T. Berlijn, P. C. Snijders, O. Delaire, H.-D. Zhou, T. A. Maier, H.-B. Cao, S.-X. Chi, M. Matsuda, Y. Wang, M. R. Koehler, P. R. C. Kent, and H. H. Weitering, *Phys. Rev. Lett.* **118**, 077201 (2017).
- [67] Z. H. Zhu, J. Stempfer, R. R. Rao, C. A. Occhialini, J. Pellicciari, Y. Choi, T. Kawaguchi, H. You, J. F. Mitchell, Y. Shao-Horn, and R. Comin, *Phys. Rev. Lett.* **122**, 017202 (2019).
- [68] D. N. Argyriou, J. F. Mitchell, P. G. Radaelli, H. N. Bordallo, D. E. Cox, M. Medarde, and J. D. Jorgensen, *Phys. Rev. B* **59**, 8695 (1999).
- [69] J.-S. Zhou, C.-Q. Jin, Y.-W. Long, L.-X. Yang, and J. B. Goodenough, *Phys. Rev. Lett.* **96**, 046408 (2006).
- [70] B. Chamberland, *Solid State Commun.* **5**, 663 (1967).
- [71] J.-S. Zhou, J. A. Alonso, J. Sanchez-Benitez, M. T. Fernandez-Diaz, R. Martinez-Coronado, L.-P. Cao, X. Li, L. G. Marshall, C.-Q. Jin, and J. B. Goodenough, *Phys. Rev. B* **92**, 144421 (2015).
- [72] Y. Qian, G. Wang, Z. Li, C. Jin, and Z. Fang, *New J. Phys.* **13**, 053002 (2011).